Dynamic response of metal sandwich beams under high velocity impact by considering time inhomogeneity of the core deformation

Wen-Zheng Jiang [1], Ying Liu[1,2*], Bin Wang[3]

[1]Department of Mechanics, School of Civil Engineering, Beijing Jiaotong University, Beijing, 100044

[2] Xi'an Jiaotong University

[3]Department of Mechanical, Aerospace and Civil Engineering, Brunel University, Uxbridge, London, UK

Corresponding author:

Ying Liu

Department of Mechanics

School of Civil Engineering

Beijing Jiaotong University

Beijing 100044

Email: yliu5@bjtu.edu.cn

Tel: 86-10-51682094; Fax: 86-10-51682094

ABSTRACTS

The objective of this paper is to study the large deflection of a fully clamped sandwich beam under high-velocity impact by considering the time in-homogeneity of the core deformation. Firstly, a unified dynamic yielding criterion for metallic sandwich beams considering the mass redistribution along with the core compression is proposed. Different from the traditional yielding surface, when the core is partially densified, the yield surface is asymmetric. The well-known yielding criterion for the solid monolithic beam is a special case of our model. Moreover, a membrane factor is proposed and an analytical solution for the large deflection of the beam under blasting loading is given. Comparison of the analytical solutions with numerical ones reveals that the present analytical model improves the prediction accuracy of the high-velocity impact response of fully clamped sandwich beams. Moreover, the present analytical method can also be degenerated to predict the low velocity/energy impact response of sandwich beams.

Keywords

A. sandwich beam; A. Yield criterion; C. High-velocity; C. Large deflection

1. Introduction

Due to the light weight and high specific stiffness, sandwich structure is widely used in various important equipment, and attracts more and more attention. How to accurately predict the dynamic performance of the sandwich beams is always the frontier.

Fleck and Deshpande [1] separated the responses of the beams into three stages, and analyzed

the responses of the beams under blasting loading. Ashby [2] and Tan *et al*. [3] simulated the deformation of the foam structure by using ideal rigid-plastic locking model. Then, Lopatnikov *et al*. [4,5] extended their work by considering ideal locking elastic-plastic model. Later, Radford *et al*. [6] gives the peak and average stresses of the foam under impact loading. In 2007, Tillbrook *et al*. [7] measured the stresses on both the front and rear faces of the square-honeycombs by using a direct impact Kolsky bar. The experimental results show that under higher impact velocities, plastic wave propagation within the core results in the stress increase in the front face along with the increase of the velocity; whilst the rear face stresses remain approximately constant. Barnes *et al*. [8] and Gaitanaros *et al*. [9] presented the results of a study of the crushing behavior of open-cell Al foams under impact. They also found the in-homogeneous stress distribution in the sandwich beam. The stress behind the shocks was found to increase as square of velocity. The stress in front of the shock remained at a constant level that approximately corresponded to the initiation stress recorded in quasi-static crushing experiments.

Without considering the coupling responses of the cover sheets and foam core, Qin and Wang [10,11] derived a yielding criterion for geometrically symmetric metal sandwich structures incorporating the effect of core strength. They obtained an analytical solution for the large deflection of a slender symmetric metal foam core sandwich beam with axial restraints under transverse loading by a flat punch. Based on that criterion, Qin and Wang [12] and Qin *et al*. [13] investigated the impulsive response of fully clamped symmetric metal sandwich beams by using the membrane factor method, in which interaction of bending and stretching is considered. Then Qin and Zhang [14,15] analyzed the low-velocity impact responses of fully clamped slender sandwich beams with geometrically asymmetric cross-section struck by a heavy mass. The

yielding criteria for asymmetric sandwich structures were presented, and provided acceptable predictions of the low-velocity impact of fully clamped geometrically asymmetric slender sandwich beams.

However, their models are based on the low-velocity impact or quasi-static loading. Moreover, as aforementioned, the stress distributions on the face sheets and in the core are velocity dependent. Under a high-velocity impact, the cellular core displays local deformation characteristics. As a result, the mass is reassigned in the space, which causes the time heterogeneity of the deformation. To per authors' knowledge, this time heterogeneity due to the local deformation of the cellular core under high-speed impact has not yet been fully considered in the previous modeling. The dynamic yielding criteria considering the time heterogeneity for sandwich structure under high-speed impact should be further investigated.

The objective of this paper is to establish the dynamic yielding criteria for a slender sandwich beam by including the time heterogeneity of the cellular core during the deformation under the high-velocity impact. A membrane factor for the dynamic responses of a metallic sandwich beam under the high-velocity impact is proposed to incorporating the large deformation effect. Based on the proposed dynamic yielding criteria and the membrane factor, the dynamic deformation of a fully clamped slender sandwich beam under blasting loading is predicted and corresponding comparison with the previous theoretical results are made. At last, the conclusion is given.

2. Dynamic yielding criterion with time in-homogeneity for sandwich beams

As shown in Fig. 1, we consider a slender metallic foam core sandwich beam with a rectangular cross-section and axial constraints. The sandwich beam is transversely loaded at its front face sheet by a blasting impulse. We assumed that the the front and back layers metals obey the

rigid-perfectly plastic law with the yield strength are σ_f. During the deformation, the cellular foam core is gradually densified from the impact end to the opposite end. We ignore the shear force, and assume that the metal foam core with thickness C, z is the densification region, which is linearly varied with respect to the time ($z = vt$. $0 \le z \le (1-\varepsilon_D)\mathrm{C}$). The metal foam cores obey the yield strength σ_c is molded as rigid-perfectly-plastic-locking *RPPL* material (Fig. 2). Geometric sizes and material characteristics can affect the composition of the structure. b is the width of the cross-section, and assume that the width is unit length.

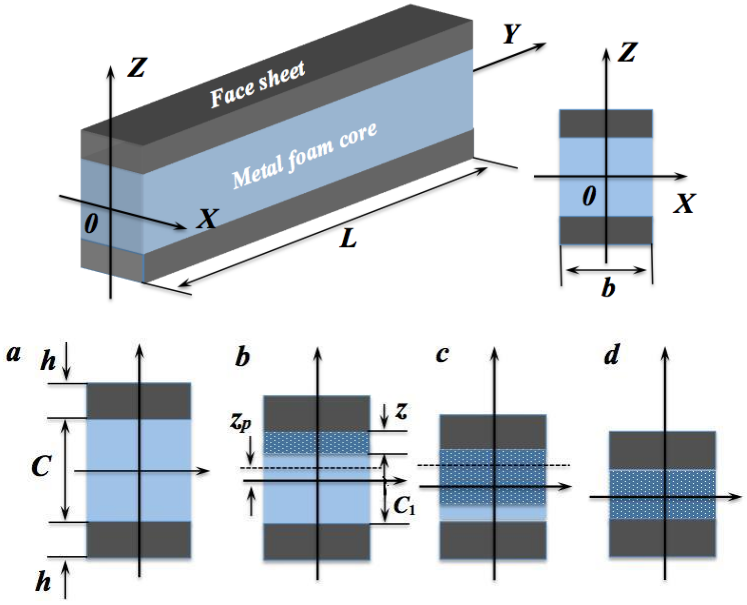

Fig. 1 Original and deformed cross-sections of the sandwich beam.

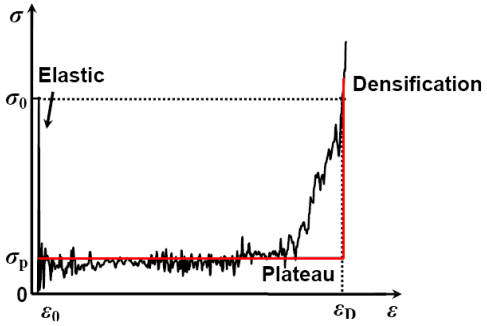

Fig. 2 Typical dynamic stress-strain curves for the foam. The red line corresponds to rigid ideally-plastic-locking model.

Herein, we define z_p as the plastic neutral surface, which is marked out by dash dot line shown in Fig. 3. Then we have

$$\int_{\frac{C-\lambda_\varepsilon z}{2}-h}^{z_p}\sigma(z)dz=\int_{z_p}^{\frac{C-\lambda_\varepsilon z}{2}+h}\sigma(z)dz\,, \tag{1}$$

Where $\sigma(z)$ is the yielding strength of the materials, and $\lambda_\varepsilon=\varepsilon_D/(1-\varepsilon_D)$. ε_D is the densification strain. Along with the densification of the foam core, the plastic neutral surface gradually moves away from *X*-axis. When $z=C(1-\varepsilon_D)/2$, z_p has the maximum value. Then along with the further compression, the plastic neutral surface moves back to *X*-axis and coincides with *X*-axis when the core is fully densified, that is,

$$z_p=\begin{cases}\dfrac{\lambda_\varepsilon z}{2}, & 0\le z\le\dfrac{C(1-\varepsilon_D)}{2}\\[2ex] \dfrac{(C-\lambda_\varepsilon z-z)\varepsilon_D}{2}. & \dfrac{C(1-\varepsilon_D)}{2}\le z\le C(1-\varepsilon_D)\end{cases} \tag{2}$$

When $x=C(1-\varepsilon_D)/2$, the interface between the compression region and the uncompressed region coincides with the neutral axis. As shown in Fig. 3, during the compression, the axial force *N* and the bending moment *M* could be expressed according the position of the neutral axis as follows.

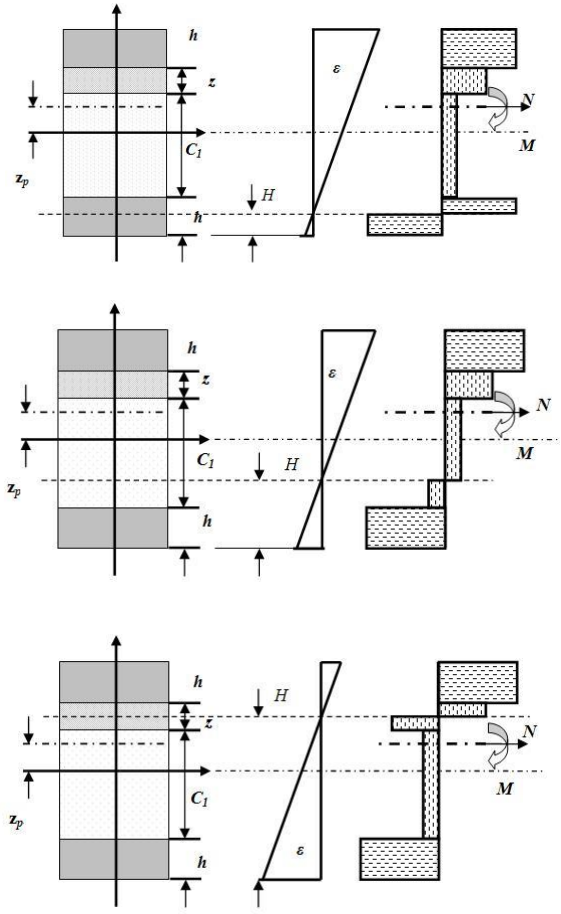

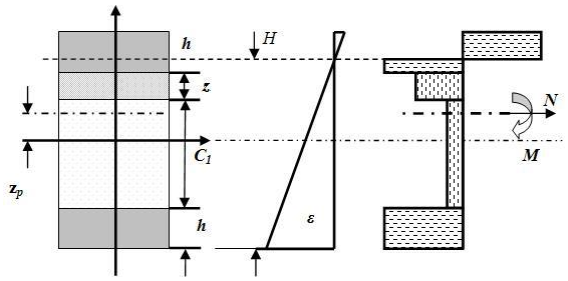

Fig.3 Distributions of the strain and stress on the cross-section of multilayer beam under bending moment and axial force.

2.1. Case I: the plastic neutral axis moves away from *X*-axis, that is, $z \le C(1-\varepsilon_D)/2$ **with** $z_p=\lambda_\varepsilon z/2$.

The resultants of the axial force N and the bending moment M for different values of η can be expressed as

$$N=\int_A \sigma(Z)dA=\begin{cases}\sigma_c C+2\sigma_f[h-\eta(2h+C-\lambda_\varepsilon z)], \\ 0\le\eta\le h/(2h+C-\lambda_\varepsilon z) \\ \sigma_c[C-2\eta(2h+C-\lambda_\varepsilon z)+2h], \\ h/(2h+C-\lambda_\varepsilon z)\le\eta\le\dfrac{h+C-\lambda_\varepsilon z-z}{2h+C-\lambda_\varepsilon z} \\ -\sigma_c C-\dfrac{2\sigma_c}{1-\varepsilon_D}[\eta(2h+C-\lambda_\varepsilon z)-(C+h-\lambda_\varepsilon z)], \\ \dfrac{h+C-\lambda_\varepsilon z-z}{2h+C-\lambda_\varepsilon z}\le\eta\le\dfrac{h+C-\lambda_\varepsilon z}{2h+C-\lambda_\varepsilon z} \\ -\sigma_c C-2\sigma_f[h-(1-\eta)(2h+C-\lambda_\varepsilon z)], \\ (h+C-\lambda_\varepsilon z)/(2h+C-\lambda_\varepsilon z)\le\eta\le 1\end{cases}$$

$$\frac{N}{N_p}=\begin{cases}\dfrac{\bar\sigma+2[\bar h-\eta\bar r]}{\bar\sigma+2\bar h}, & 0\le\eta\le\dfrac{h}{2h+C-\lambda_\varepsilon z} \\ \dfrac{\bar\sigma[1-2\eta\bar r+2\bar h]}{\bar\sigma+2\bar h}, & \dfrac{h}{2h+C-\lambda_\varepsilon z}\le\eta\le\dfrac{h+C-\lambda_\varepsilon z-z}{2h+C-\lambda_\varepsilon z} \\ \dfrac{-\bar\sigma-2\bar\sigma[\bar r(\eta-1)+\bar h]/(1-\varepsilon_D)}{\bar\sigma+2\bar h}, & \dfrac{h+C-\lambda_\varepsilon z-z}{2h+C-\lambda_\varepsilon z}\le\eta\le\dfrac{h+C-\lambda_\varepsilon z}{2h+C-\lambda_\varepsilon z} \\ \dfrac{-\bar\sigma-2[\bar r(\eta-1)+\bar h]}{\bar\sigma+2\bar h}, & \dfrac{h+C-\lambda_\varepsilon z}{2h+C-\lambda_\varepsilon z}\le\eta\le 1\end{cases} \tag{3}$$

$$
M=\int_A \sigma(\mathrm{Z})ZdA=\begin{cases}
\int_{-z_p-h-(C-\lambda_\varepsilon z)/2+H}^{-z_p-h-(C-\lambda_\varepsilon z)/2}-\sigma_f ZdA+\int_{-z_p-(C-\lambda_\varepsilon z)/2}^{-z_p-(C-\lambda_\varepsilon z)/2-h+H}\sigma_f ZdA+\int_{-z_p-(C-\lambda_\varepsilon z)/2}^{(C-\lambda_\varepsilon z)/2-z_p-z}\sigma_c ZdA \\
+\int_{(C-\lambda_\varepsilon z)/2-z_p-z}^{(C-\lambda_\varepsilon z)/2-z_p}\frac{\sigma_c}{1-\varepsilon_D}ZdA+\int_{(C-\lambda_\varepsilon z)/2-z_p}^{h+(C-\lambda_\varepsilon z)/2-z_p}\sigma_f ZdA, \\
0\le\eta\le h/(2h+C-\lambda_\varepsilon z) \\
\int_{-z_p-(C-\lambda_\varepsilon z)/2-h}^{-z_p-(C-\lambda_\varepsilon z)/2}-\sigma_f ZdA+\int_{-z_p-(C-\lambda_\varepsilon z)/2}^{-z_p-(C-\lambda_\varepsilon z)/2-h+H}-\sigma_c ZdA+\int_{-z_p-(C-\lambda_\varepsilon z)/2-h+H}^{(C-\lambda_\varepsilon z)/2-z_p-z}\sigma_c ZdA \\
+\int_{(C-\lambda_\varepsilon z)/2-z_p-z}^{(C-\lambda_\varepsilon z)/2-z_p}\frac{\sigma_c}{1-\varepsilon_D}ZdA+\int_{(C-\lambda_\varepsilon z)/2-z_p}^{h+(C-\lambda_\varepsilon z)/2-z_p}\sigma_f ZdA, \\
h/(2h+C-\lambda_\varepsilon z)\le\eta\le(h+C-\lambda_\varepsilon z-z)/(2h+C-kx) \\
\int_{-z_p-(C-\lambda_\varepsilon z)/2-h}^{-z_p-(C-\lambda_\varepsilon z)/2}-\sigma_f ZdA+\int_{-z_p-(C-\lambda_\varepsilon z)/2}^{(C-\lambda_\varepsilon z)/2-z_p-z}-\sigma_c ZdA+\int_{(C-\lambda_\varepsilon z)/2-z_p-z}^{-z_p-h-(C-\lambda_\varepsilon z)/2+H}-\frac{\sigma_c}{1-\varepsilon_D}ZdA \\
+\int_{-z_p-h-(C-\lambda_\varepsilon z)/2+H}^{(C-\lambda_\varepsilon z)/2-z_p}\frac{\sigma_c}{1-\varepsilon_D}ZdA+\int_{(C-\lambda_\varepsilon z)/2-z_p}^{h+(C-\lambda_\varepsilon z)/2-z_p}\sigma_f ZdA, \\
(h+C-\lambda_\varepsilon z-z)/(2h+C-\lambda_\varepsilon z)\le\eta\le(h+C-\lambda_\varepsilon z)/(2h+C-\lambda_\varepsilon z) \\
\int_{-z_p-(C-\lambda_\varepsilon z)/2-h}^{-z_p-(C-\lambda_\varepsilon z)/2}-\sigma_f zdA+\int_{-z_p-(C-\lambda_\varepsilon z)/2}^{(C-\lambda_\varepsilon z)/2-z_p-z}-\sigma_c ZdA+\int_{(C-\lambda_\varepsilon z)/2-z_p-z}^{(C-\lambda_\varepsilon z)/2-z_p}-\frac{\sigma_c}{1-\varepsilon_D}ZdA \\
+\int_{(c-\lambda_\varepsilon z)/2-z_p}^{-z_p-h-(c-\lambda_\varepsilon z)/2+H}-\sigma_f ZdA+\int_{-z_p-h-(C-\lambda_\varepsilon z)/2+H}^{h+(C-\lambda_\varepsilon z)/2-z_p}\sigma_f ZdA, \\
(h+C-\lambda_\varepsilon z)/(2h+C-\lambda_\varepsilon z)\le\eta\le 1
\end{cases}
$$

$$
\frac{M}{M_p}=\begin{cases}
\dfrac{-\eta^2\bar{r}^2+\eta(\bar{r}^2+\bar{k}\bar{r})-\bar{k}\bar{h}+\dfrac{\bar{\sigma}\bar{k}(\bar{l}-1)}{2}}{\bar{\sigma}/4+\bar{h}(\bar{r}-\bar{h})}, & 0\le\eta\le h/(2h+C-\lambda_\varepsilon z) \\
\dfrac{\bar{h}(\bar{r}-\bar{h})+\bar{\sigma}[-\eta^2\bar{r}^2+\eta\bar{r}(2\bar{h}+1)-\bar{h}^2-\bar{h}+\dfrac{\bar{k}(\bar{l}-1)}{2}]}{\bar{\sigma}/4+\bar{h}(\bar{r}-\bar{h})}, & \\
\qquad h/(2h+C-\lambda_\varepsilon z)\le\eta\le\dfrac{h+C-\lambda_\varepsilon z-z}{2h+C-\lambda_\varepsilon z} \\
\dfrac{\bar{h}(\bar{r}-\bar{h})+\bar{\sigma}[\dfrac{-\eta^2\bar{r}^2+\eta\bar{r}(1+2\bar{h})-\bar{h}^2-\bar{h}+\bar{k}(2\bar{h}-\bar{r}-\bar{l})/2}{1-\varepsilon_D}]}{\bar{\sigma}/4+\bar{h}(\bar{r}-\bar{h})}, & \\
\qquad \dfrac{h+C-\lambda_\varepsilon z-z}{2h+C-\lambda_\varepsilon z}\le\eta\le\dfrac{h+C-\lambda_\varepsilon z}{2h+C-\lambda_\varepsilon z} \\
\dfrac{-\eta^2\bar{r}^2+\eta(\bar{r}^2+\bar{k}\bar{r})+\bar{k}(-\bar{r}+\bar{h})+\dfrac{\bar{\sigma}\bar{k}(1-\bar{l})}{2}}{\bar{\sigma}/4+\bar{h}(\bar{r}-\bar{h})}, & \dfrac{h+C-\lambda_\varepsilon z}{2h+C-\lambda_\varepsilon z}\le\eta\le 1
\end{cases}
\tag{4}
$$

where η is the neutral surface measured from the bottom face sheet, which is denoted by $H=\eta\times(2h+C-\lambda_\varepsilon z)$. $\bar{z}=z_p/C$, $\bar{h}=h/C$, $\bar{\lambda}_\varepsilon=\lambda_\varepsilon z/C$, $\bar{r}=\left(2h+C-\lambda_\varepsilon z\right)/C$, $\bar{l}=\left(C-z-\lambda_\varepsilon z\right)/C$, the fully plastic membrane force is $N_p=\sigma_c C+2\sigma_f h$, the fully plastic bending moment is $M_p=\sigma_c C^2/4+\sigma_f h(h+C-\lambda_\varepsilon z)$, $\bar{\sigma}=\sigma_c/\sigma_f$, $N_pC/M_p=4(\bar{\sigma}+2\bar{h})/\left[\bar{\sigma}+4\bar{h}(\bar{r}-\bar{h})\right]$.

Eliminating the parameter η from Eqs. (3) and (4) and using the well-known Tresca-yield criterion,

we have the space (*M*, *N*) is with the form

$$\begin{cases} m+\dfrac{(\bar{\sigma}+2\bar{h})^2(n+1)^2}{4E_1}+\dfrac{(\bar{\lambda}_\varepsilon-\bar{r})(\bar{\sigma}+2\bar{h})(n+1)}{2E_1}+C_1=0, & -1\le n\le -n_1 \\ m+\dfrac{(\bar{\sigma}+2\bar{h})^2(1-\varepsilon_D)n^2}{4\bar{\sigma}E_1}-\dfrac{(\bar{\sigma}+2\bar{h})(\varepsilon_D-2\bar{\lambda}_\varepsilon)n}{2E_1}+C_2=0, & -n_1\le n\le n_2 \\ m+\dfrac{(\bar{\sigma}+2\bar{h})^2 n^2}{4\bar{\sigma}E_1}+C_3=0, & n_2\le n\le n_1 \\ m+\dfrac{(\bar{\sigma}+2\bar{h})^2(n-1)^2}{4E_1}+\dfrac{(\bar{r}+\bar{\lambda}_\varepsilon)(\bar{\sigma}+2\bar{h})(n-1)}{2E_1}+C_4=0, & n_1\le n\le 1 \end{cases} \tag{5}$$

where $m=M/M_P$, $n=N/N_P$, $n_1=\bar{\sigma}/\left(\bar{\sigma}+2\bar{h}\right)$, and $n_2=\left[-\bar{\sigma}+2\bar{\sigma}\bar{z}/(1-\varepsilon_D)\right]/\left(\bar{\sigma}+2\bar{h}\right)$,

$E_1=\bar{\sigma}/4+\bar{h}(\bar{r}-\bar{h})$, $C_1=-\left[2\bar{\lambda}_\varepsilon\bar{h}(1-\varepsilon_D)+\bar{\sigma}\bar{\lambda}_\varepsilon\bar{z}\right]/\left[2(1-\varepsilon_D)E_1\right]$,

$C_2=\left[4\bar{h}(\bar{h}-\bar{r})+4\bar{\sigma}\bar{\lambda}_\varepsilon-\bar{\sigma}\left(1+\varepsilon_D\right)-2\bar{\sigma}\bar{\lambda}_\varepsilon\bar{z}/(1-\varepsilon_D)\right]/4E_1$, $C_3=\left[4\bar{h}(\bar{h}-\bar{r})-\bar{\sigma}-2\bar{\sigma}\bar{\lambda}_\varepsilon\left(\bar{l}-1\right)\right]/4E_1$,

$C_4=\left[2\bar{\lambda}_\varepsilon\bar{h}+\bar{\sigma}\bar{\lambda}_\varepsilon(1-\bar{l})\right]/2E_1$.

If the core strength is equal to that of the face-sheets, that is, $\bar{\sigma}=1$, $\varepsilon_D=0$, $\bar{k}=0$, $\bar{r}=1+2\bar{h}$, $\bar{l}=1$, Eq. (5) degenerates to the well-known yielding criterion for solid monolithic beam with rectangular cross-section [16], that is,

$$|m|+n^2=1. \tag{6}$$

2.2. Case II: the plastic neutral axis moves back to *X*-axis, that is, $z>C(1-\varepsilon_D)/2$ with $z_p=(C-\lambda_\varepsilon z-z)\varepsilon_D/2$.

The resultants of the bending moment *M* for different values of η can be expressed as

$$M=\int_A \sigma Z dA=\begin{cases}\sigma_f[-H^2+H(2h+C-\lambda_\varepsilon \mathrm{z})+\varepsilon_D(C-\lambda_\varepsilon \mathrm{z}-z)(H-h)] \\ -\dfrac{\sigma_c\lambda_\varepsilon \mathrm{z}(z+\lambda_\varepsilon \mathrm{z}-C)}{2}-\sigma_c C\dfrac{\varepsilon_D(C-\lambda_\varepsilon \mathrm{z}-z)}{2}, \\ 0\le\eta\le h/(2h+C-\lambda_\varepsilon \mathrm{z}) \\ \sigma_f h(h+C-\lambda_\varepsilon \mathrm{z})+\sigma_c(\dfrac{\lambda_\varepsilon \mathrm{z}(C-z-\lambda_\varepsilon \mathrm{z})}{2}-(H-h)^2+(H-h)(C-\lambda_\varepsilon \mathrm{z}) \\ -(C+2h-2H)\dfrac{\varepsilon_D(C-\lambda_\varepsilon \mathrm{z}-z)}{2}), \\ h/(2h+C-\lambda_\varepsilon \mathrm{z})\le\eta\le\dfrac{h+C-\lambda_\varepsilon \mathrm{z}-z}{2h+C-\lambda_\varepsilon \mathrm{z}} \\ \sigma_f h(h+C-\lambda_\varepsilon \mathrm{z})+\sigma_c(\dfrac{-(H-h)^2+(H-h)(C-\lambda_\varepsilon \mathrm{z})}{1-\varepsilon_D}-\dfrac{\lambda_\varepsilon \mathrm{z}(C-z-\lambda_\varepsilon \mathrm{z})}{2} \\ -\lambda_\varepsilon(C-z-\lambda_\varepsilon \mathrm{z})\dfrac{\varepsilon_D(C-\lambda_\varepsilon \mathrm{z}-z)}{2}-\dfrac{(C+2h-\lambda_\varepsilon \mathrm{z}-2H)\dfrac{\varepsilon_D(C-\lambda_\varepsilon \mathrm{z}-z)}{2}}{1-\varepsilon_D}), \\ (h+C-\lambda_\varepsilon \mathrm{z}-z)/(2h+C-\lambda_\varepsilon \mathrm{z})\le\eta\le(h+C-\lambda_\varepsilon \mathrm{z})/(2h+C-\lambda_\varepsilon \mathrm{z}) \\ \sigma_f[-H^2+\eta(2h+C-\lambda_\varepsilon \mathrm{z})^2+\varepsilon_D(C-\lambda_\varepsilon \mathrm{z}-z)(H-r+h)] \\ -\dfrac{\sigma_c\lambda_\varepsilon \mathrm{z}(C-z-\lambda_\varepsilon \mathrm{z})}{2}+\sigma_c C\dfrac{\varepsilon_D(C-\lambda_\varepsilon \mathrm{z}-z)}{2}, \\ \dfrac{h+C-\lambda_\varepsilon \mathrm{z}}{2h+C-\lambda_\varepsilon \mathrm{z}}\le\eta\le 1\end{cases} \tag{7}$$

Similarly, we have the yield criteria in space (M, N) are

$$\begin{cases} m+\dfrac{(\bar\sigma+2\bar h)^2(n+1)^2}{4E_1}+\dfrac{(\varepsilon_D\bar l-\bar r)(\bar\sigma+2\bar h)(n+1)}{2E_1}+D_1=0, & -1\le n\le -n_1 \\ m+\dfrac{(\bar\sigma+2\bar h)^2(1-\varepsilon_D)n^2}{4\bar\sigma E_1}+\dfrac{(\varepsilon_D\bar l+\bar\lambda_\varepsilon-\varepsilon_D)(\bar\sigma+2\bar h)n}{2E_1}+D_2=0, & -n_1\le n\le n_2 \\ m+\dfrac{(\bar\sigma+2\bar h)^2n^2}{4\bar\sigma E_1}+\dfrac{(\bar\sigma+2\bar h)(\varepsilon_D\bar l-\bar\lambda_\varepsilon)n}{2E_1}+D_3=0, & n_2\le n\le n_1 \\ m+\dfrac{(\bar\sigma+2\bar h)^2(n-1)^2}{4E_1}+\dfrac{(\bar r+\varepsilon_D\bar l)(\bar\sigma+2\bar h)(n-1)}{2E_1}+D_4=0, & n_1\le n\le 1 \end{cases} \tag{8}$$

where $D_1=\left[-2\varepsilon_D\overline{lh}-\bar\sigma\bar l(\varepsilon_D-\bar\lambda_\varepsilon)\right]/2E_1$, $D_2=\left[4\bar h(\bar h-\bar r)-\bar\sigma(1+\varepsilon_D)+2\bar\sigma\bar\lambda_\varepsilon(1+\bar l)\right]/4E_1$, $D_3=\left[4\bar h(\bar h-\bar r)-\bar\sigma+2\bar\sigma\bar\lambda_\varepsilon(1-\bar l)\right]/4E_1$, $D_4=\left[2\varepsilon_D\overline{lh}+\bar\sigma\bar l(\varepsilon_D-\bar\lambda_\varepsilon)\right]/2E_1$.

Based on Eqs. (5) and (8), Fig. 4a shows the predicted dynamic yield surfaces for the metal sandwich along with the compression. When T=0, that is, the yield surface is just the surface predicted by Qin and Wang [11], shown as Fig. 4b. It is noticed that along with the core compression, the yield surface will be gradually reduced. After the core thickness keeps constant (core densified or the velocities of the face sheets arriving the same value), the yield surface is degenerated to the one given by Qin and Wang [12]. Seen as Fig. 4b, when the core is partially densified, the yield surface is asymmetric; whilst when the core is fully densified, the yield surface is identical to the initial one, which is symmetry. The variation of the dynamic yielding surface

indicates that if the core inhomogeneity is ignored, the model may less prediction the deformation of the sandwich beam.

It is seen that the present yield criterion considers the core deformation and the variation of the beam cross section during the compression. The variation of the neutral axis on the responses of the metallic sandwich is included. The previous yielding criteria for the deformation of sandwich beams or for solid monolithic beams are just the special cases of our results. It is also demonstrated that the quasi-static yield criterion becomes less accurate for the sandwich beam under the high-velocity impact when the core is compressed.

In what follows, the yield criterion will be employed to derive the analytical solutions for the large deflection of fully clamped sandwich beams with a metal foam core, in which the interaction of bending and stretching is considered. Especially, during the densification of the core, the bending moment and the axial force of the sandwich beam could be determined as needed.

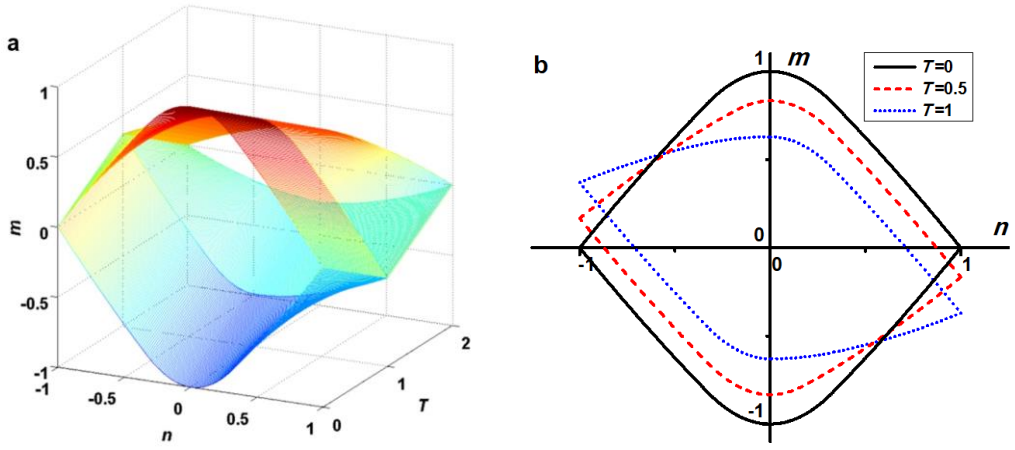

Fig. 4 Dynamic yield surfaces for the compressed sandwich beam along with the compression.

3. Analytical model for sandwich beams under blasting loading

Seen as Fig. 5, the sandwich beam length is $2L$ and core thickness is C, the thicknesses of the front and back face-sheets are h_f and h_b, respectively. The core density is ρ_c, the uniaxial yield

strengths of the transverse and longitudinal directions are σ_t and σ_l. (Assume that the tensile and compressive yield values are equal.) The core has a nominal compressive densification strain, ε_D. The face-sheet material has a density ρ_f and obeys to the rigid-ideally plastic model with a tensile strength σ_Y. The boundary conditions for the sandwich beam are shown in Fig. 5. The back face is fully clamped at two outer supports while only the lateral displacements of the front face are constrained. These boundary conditions were the same as Liang *et al*. [17] (considered to be representative of ship hulls). This sandwich beam is impulsively loaded with an impulse I per unit length applied uniformly to the front face-sheet of the sandwich beam.

We consider the core with micro-inertial or shock wave effects and assume that the transverse compressive stress σ_t loads at the back face, the compressive stress σ_m loads at the front face, decelerating the front face as illustrated in Fig. 6. After the impulse impacting, the front face gets the velocity. In order to keep balance, a disturbance is propagated along the beam from the fixed ends to the midpoint and the core is gradually compressed, which is displayed in Fig. 7. Then the front face begins to decelerate, and the back face begins to accelerate, that is, phase I, Fig. 7a, and phase II, Fig. 7c. The front and back faces are coupled with each other in phases I and II. The core compression ends at time $t = t_{eq}$ after which the beams deform as a system (phase III, Fig. 7e).

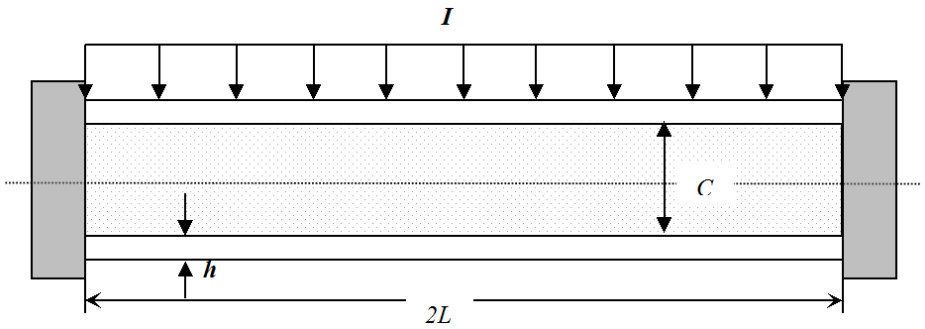

Fig. 5 Geometry of the sandwich beam and schematic of the problem under consideration.

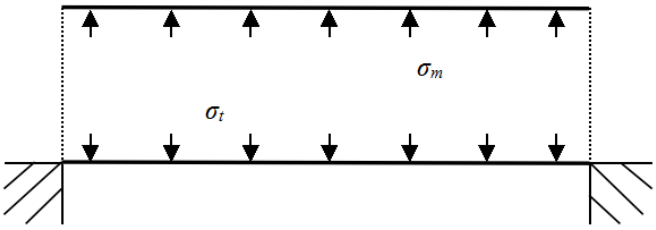

Fig. 6 A sketch summarizing the model of the sandwich beam subject to impulse loading.

3.1. Governing equations prior to the equalization of the face-sheet velocities (Coupling Response)

The governing equations for the motion of the front and back faces by assuming that the two face-sheets deflect independently. Employing the lumped mass approximation, the mass per unit length of the front and back faces are

$$m_f = h_f \rho_f + \rho_c C/2 \, , m_b = h_b \rho_b + \rho_c C/2 \, . \tag{9}$$

With an impulse I applied uniformly to the front face of the sandwich beam, the initial velocity v_0 of the front face in this lumped mass model follows as

$$v_0 = \frac{I}{m_f} \, . \tag{10}$$

An extensive series of experiments had been performed by using foam impact in order to determine the functional relationship between pressure history and impact velocity. The theoretical prediction of peak pressure is given as Radford *et al*. [6]

$$\sigma_{peak} = \sigma_t + \rho_c V_0^2 / \varepsilon_D \, , \tag{11}$$

which agrees well with the experimental measurements.

The experimental data for the mean pressure is more accurately represented by the empirical fit,

$$\sigma_m = \sigma_t + 0.66 \rho_c V_0^2 / \varepsilon_D \, . \tag{12}$$

3.1.1. Front face

The front face begins to decelerate with the initial velocity v_0. We have the velocity and deflection

of the front face

$$v_f(t) = v_0 - \frac{\sigma_m}{m_f} t, \tag{13}$$

$$w_f(t) \equiv \varepsilon(t) c = v_0 t - \frac{\sigma_m}{2m_f} t^2. \tag{14}$$

When $\varepsilon(t) = \varepsilon_D$, full densification of the core will occur at a time t_D, that is,

$$t_D = \frac{m_f v_0}{\sigma_m} - \sqrt{\left(\frac{m_f v_0}{\sigma_m}\right)^2 - \frac{2m_f \varepsilon_D c}{\sigma_m}}.$$

3.1.2. Back face

Here we use the finite deflection solution along the lines of the impulsive solution of Tilbrook *et al*. [18] . There are three cases as follow:

Case I: High strength core, that is, $\sigma_t > 3(\sigma_Y h_b^2 / L^2)$;

In the initial phase I (Fig. 7a), the mid-span velocity and the deflection of the back face are

$$v_b(t) = \frac{\sigma_t}{m_b} t, \tag{15}$$

$$w_b(t) = \frac{\sigma_t}{2m_b} t^2. \tag{16}$$

A disturbance propagates from the central point to the fixed ends. When the plastic hinge arrives at the midpoint, we have $\xi = L$, that is, $t = t_I$, with v_b^I and w_b^I, the first phase ends.

In the phase II, the plastic hinges are fixed at the mid-span and the ends of the beam, as sketched in Fig. 5c, the mid-span deflection and the velocity of the back face are

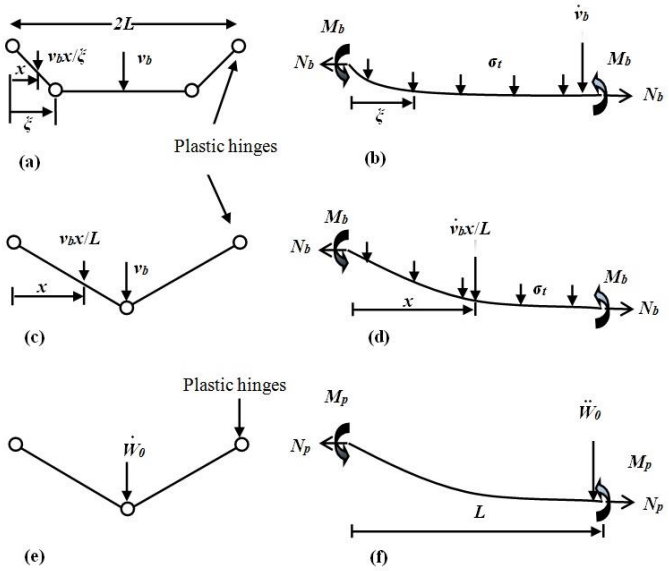

Fig. 7 (a) Velocity profile of the back face in phase I, (b) a free-body diagram of the left half back beam in phase I; (c) Velocity profile of the back face in phase II, and (d) a free body diagram of the left half back beam in phase II; (e) Velocity profile of the sandwich phase, and (f) a free body diagram of the half beam.

$$w_b(t) = \frac{v_b^I}{\omega}\sin[\omega(t-t_I)] - \frac{4M_b}{N_b}\cos[\omega(t-t_I)] + \left(\frac{4M_b}{N_b} + w_b^I\right), \tag{17}$$

$$v_b = \dot{w}_b = v_b^I\cos[\omega(t-t_I)] + \frac{4M_b}{N_b}\omega\sin[\omega(t-t_I)]. \tag{18}$$

where $\omega = \frac{1}{L}\sqrt{\frac{3N_b}{m_b}}$, $M_b = \sigma_Y h_b^2/4$, $N_b = \sigma_Y h_b$.

When the back face begins to decelerate, the acceleration is $\dot{v}_b = 0$ and the time is t_{bd}. From Eq. (18), we have,

$$t_{bd} = t_I + \frac{1}{\omega}\tan^{-1}\left(\frac{4M_b\omega}{N_b v_b^I}\right). \tag{19a}$$

When $v_b = 0$, the back face arrests at the time

$$t_{bs} = t_I + \frac{1}{\omega}\left[\frac{\pi}{2} + \tan^{-1}\left(\frac{4M_b\omega}{N_b v_b^I}\right)\right]. \tag{19b}$$

Case II: Intermediate strength core, that is, $\sigma_Y h_b^2/L^2 < \sigma_t \le 3(\sigma_Y h_b^2/L^2)$;

Then, the mid-span deflection and the velocity of the back face are given by

$$w_b(t) = \left(\frac{\sigma_t L^2 - 4M_b}{2N_b}\right)(1-\cos\omega t), \tag{20a}$$

$$v_b(t) = \omega\left(\frac{\sigma_t L^2 - 4M_b}{2N_b}\right)\sin\omega t\,. \tag{20b}$$

And the times t_{bd} and t_{bs} are

$$t_{bd} = \frac{\pi}{2} L\sqrt{\frac{m_b}{3N_b}}\,, \tag{21a}$$

$$t_{bs} = \pi L\sqrt{\frac{m_b}{3N_b}}\,. \tag{21b}$$

Case III: Low strength core, that is, $\sigma_t \le \sigma_Y h_b^2 / L^2$.

In this case, the strength of the core is so soft that the back face will not deform. Thus, within the rigid-ideally plastic idealization, the back face does not deflect due to the pressure σ_t exerted by the core, and we have $\dot{w}_b = w_b = 0$.

Now the core compression ends when the core has been densified at $t = t_D$, or when the front and back face-sheet velocities are equal at the mid-span, whichever occurs first. The detailed governing equations are given in Appendix A.

3.2. The membrane factor for the sandwich phase of motion (Overall response)

The core compression ends at time $t = t_{eq}$ or $t = t_D$, after which the beams deform as a system. Yu *et al*. [19] proposed a 'membrane factor' to consider the effect of axial force on the energy dissipation of a solid monolithic beam with large deflection. Here this method is extended to solve the dynamic response of large deflection of a fully clamped sandwich beam subjected to the high velocity impact. We assume that the longitudinal extension of the sandwich beam is

$$e = e_1 + e_2\,. \tag{22}$$

where e_1 and e_2 are the axial extensions concentrated at the ends of the left-hand portion (see,

Fig. 7f). The rate of the angular rotation at the hinges located at x=0 and x=L. The total elongation of the left-hand part of the sandwich beam and the angular rotation are

$$e \approx \frac{W_0^2}{2L_0}, \kappa \approx \frac{W_0}{L_0}, \tag{23}$$

where L_0 is the half span length of the sandwich beam. W_0 is the mid-span deflection of the sandwich beam.

According to the associated flow rule, we have

$$\frac{\dot{e}}{\dot{\kappa}} = \frac{\dot{e}_1 + \dot{e}_2}{\dot{\kappa}} = -\frac{dM}{dN} = W_0. \tag{24}$$

Using the associated flow rules of the yielding criteria given by Eqs. (5) and (8), the relations between the non-dimensional axial force n and the mid-span deflection W_0 then can be expressed according to the positions of the plastic hinges. If the plastic hinges are at the mid-span, we have

$$W_{11} = \begin{cases} \dfrac{(\bar{\sigma}+2\bar{h})n}{2\bar{\sigma}} C, & 0 \le n \le n_1 \\ \dfrac{(\bar{\sigma}+2\bar{h})(n-1)+(\bar{r}+\bar{\lambda}_\varepsilon)}{2} C, & n_1 \le n \le 1 \end{cases} \tag{25a}$$

$$W_{12} = \begin{cases} \dfrac{(\bar{\sigma}+2\bar{h})(1-\varepsilon_D)n+\bar{\sigma}(\varepsilon_D \bar{l}+\bar{\lambda}_\varepsilon-\varepsilon_D)}{2\bar{\sigma}} C, & 0 \le n \le n_2 \\ \dfrac{(\bar{\sigma}+2\bar{h})n+\bar{\sigma}(\varepsilon_D \bar{l}-\bar{\lambda}_\varepsilon)}{2\bar{\sigma}} C, & n_2 \le n \le n_1 \\ \dfrac{(\bar{\sigma}+2\bar{h})(n-1)+(\bar{r}+\varepsilon_D \bar{l})}{2} C, & n_1 \le n \le 1 \end{cases} \tag{25b}$$

where $W_1 = \dot{e}_1 / \dot{\kappa}$, $n_1 = \bar{\sigma} / (\bar{\sigma}+2\bar{h})$, and $n_2 = [-\bar{\sigma}+2\bar{\sigma}\bar{z}/(1-\varepsilon_D)] / (\bar{\sigma}+2\bar{h})$.

If the plastic hinges are at the supports, we have

$$W_{21} = \begin{cases} \dfrac{(\bar{\sigma}+2\bar{h})n}{2\bar{\sigma}} C, & 0 \le n \le -n_2 \\ \dfrac{(\bar{\sigma}+2\bar{h})(1-\varepsilon_D)n+\bar{\sigma}(\varepsilon_D-2\bar{\lambda}_\varepsilon)}{2\bar{\sigma}} C, & -n_2 \le n \le n_1 \\ \dfrac{(\bar{\sigma}+2\bar{h})(n-1)-(\bar{\lambda}_\varepsilon-\bar{r})}{2} C, & n_1 \le n \le 1 \end{cases} \tag{26a}$$

$$W_{22} = \begin{cases} \dfrac{(\bar{\sigma}+2\bar{h})(1-\varepsilon_D)n-\bar{\sigma}(\varepsilon_D \bar{l}+\bar{\lambda}_\varepsilon-\varepsilon_D)}{2\bar{\sigma}} C, & 0 \le n \le n_1 \\ \dfrac{(\bar{\sigma}+2\bar{h})(n-1)-(\varepsilon_D \bar{l}-\bar{r})}{2} C, & n_1 \le n \le 1 \end{cases} \tag{26b}$$

where $W_2 = \dot{e}_2 / \dot{\kappa}$.

From Eqs. (24), (25) and (26), we have the relationship between the deflection W_0 and the non-dimensional axial force n, that is,

$$W_{01}=\begin{cases}\dfrac{(\bar{\sigma}+2\bar{h})n}{\bar{\sigma}}C, & 0\le n\le -n_2\\ \dfrac{(\bar{\sigma}+2\bar{h})(2-\varepsilon_D)n+\bar{\sigma}(\varepsilon_D-2\bar{\lambda}_\varepsilon)}{2\bar{\sigma}}C, & -n_2\le n\le n_1\\ \left[(\bar{\sigma}+2\bar{h})(n-1)+\bar{r}\right]C, & n_1\le n\le 1\end{cases} \tag{27a}$$

$$W_{02}=\begin{cases}\dfrac{(\bar{\sigma}+2\bar{h})(1-\varepsilon_D)n}{\bar{\sigma}}C, & 0\le n\le n_2\\ \dfrac{(\bar{\sigma}+2\bar{h})(2-\varepsilon_D)n+\bar{\sigma}(\varepsilon_D-2\bar{\lambda}_\varepsilon)}{2\bar{\sigma}}C, & n_2\le n\le n_1\\ \left[(\bar{\sigma}+2\bar{h})(n-1)+\bar{r}\right]C. & n_1\le n\le 1\end{cases} \tag{27b}$$

Rewriting Eq. (27), we have

$$n_{01}=\begin{cases}\dfrac{\bar{w}_1\bar{\sigma}}{(\bar{\sigma}+2\bar{h})}, & 0\le \bar{w}_1\le (1-\varepsilon_D)-2\bar{z}\\ \dfrac{\bar{\sigma}(2\bar{w}_1-\varepsilon_D+2\bar{\lambda}_\varepsilon)}{(\bar{\sigma}+2\bar{h})(2-\varepsilon_D)}, & (1-\varepsilon_D)-2\bar{z}\le \bar{w}_1\le (1-\bar{\lambda}_\varepsilon)\\ 1+\dfrac{\bar{w}_1-(1+2\bar{h}-\bar{\lambda}_\varepsilon)}{(\bar{\sigma}+2\bar{h})}, & (1-\bar{\lambda}_\varepsilon)\le \bar{w}_1\le 1+2\bar{h}-\bar{\lambda}_\varepsilon\end{cases} \tag{28a}$$

$$n_{02}=\begin{cases}\dfrac{\bar{w}_2\bar{\sigma}}{(\bar{\sigma}+2\bar{h})(1-\varepsilon_D)}, & 0\le \bar{w}_2\le 2\bar{z}-(1-\varepsilon_D)\\ \dfrac{\bar{\sigma}(2\bar{w}_2-\varepsilon_D+2\bar{\lambda}_\varepsilon)}{(\bar{\sigma}+2\bar{h})(2-\varepsilon_D)}, & 2\bar{z}-(1-\varepsilon_D)\le \bar{w}_2\le (1-\bar{\lambda}_\varepsilon)\\ 1+\dfrac{\bar{w}_2-(1+2\bar{h}-\bar{\lambda}_\varepsilon)}{(\bar{\sigma}+2\bar{h})}, & (1-\bar{\lambda}_\varepsilon)\le \bar{w}_2\le 1+2\bar{h}-\bar{\lambda}_\varepsilon\end{cases} \tag{28b}$$

where $\bar{w}_1=W_{01}/C$, $\bar{w}_2=W_{02}/C$.

Substitution of Eq. (28) into Eqs. (5) and (8) leads to

$$m_1=\begin{cases}-\dfrac{\bar{\sigma}\bar{w}_1^2}{4E_1}-C_3, & 0\le \bar{w}_1\le (1-\varepsilon_D)-2\bar{z}\\ -\dfrac{\bar{\sigma}(1-\varepsilon_D)[2\bar{w}_1-\varepsilon_D+2\bar{\lambda}_\varepsilon]^2}{4E_1(2-\varepsilon_D)^2}-\dfrac{\bar{\sigma}(2\bar{\lambda}_\varepsilon-\varepsilon_D)[2\bar{w}_1-\varepsilon_D+2\bar{\lambda}_\varepsilon]}{2E_1(1-\varepsilon_D)}-C_2, & (1-\varepsilon_D)-2\bar{z}\le \bar{w}_1\le (1-\bar{\lambda}_\varepsilon)\\ -\dfrac{(\bar{w}_1-1-2\bar{h}+\bar{\lambda}_\varepsilon)^2}{4E_1}+\dfrac{(\bar{k}-\bar{r})(\bar{w}_1-1-2\bar{h}+\bar{\lambda}_\varepsilon)}{2E_1}-C_1, & (1-\bar{\lambda}_\varepsilon)\le \bar{w}_1\le 1+2\bar{h}-\bar{\lambda}_\varepsilon\end{cases} \tag{29a}$$

$$m_2=\begin{cases}-\dfrac{\bar{\sigma}\bar{w}_2^2}{4E_1(1-\varepsilon_D)}-\dfrac{(\varepsilon_D\bar{l}+\bar{\lambda}_\varepsilon-\varepsilon_D)\bar{w}_2\bar{\sigma}}{2E_1(1-\varepsilon_D)}-D_2, & 0\le \bar{w}_2\le 2\bar{z}-(1-\varepsilon_D)\\ -\dfrac{\bar{\sigma}[2\bar{w}_2-(\varepsilon_D-2\bar{\lambda}_\varepsilon)]^2}{4E_1(2-\varepsilon_D)^2}-\dfrac{\bar{\sigma}(\varepsilon_D\bar{l}-\bar{\lambda}_\varepsilon)[2\bar{w}_2-(\varepsilon_D-2\bar{\lambda}_\varepsilon)]}{2E_1(2-\varepsilon_D)}-D_3, & 2\bar{z}-(1-\varepsilon_D)\le \bar{w}_2\le (1-\bar{\lambda}_\varepsilon)\\ -\dfrac{(\bar{w}_2-1-2\bar{h}+\bar{\lambda}_\varepsilon)^2}{4E_1}-\dfrac{(\bar{r}+\varepsilon_D\bar{l})(\bar{w}_2-1-2\bar{h}+\bar{\lambda}_\varepsilon)}{2E_1}-D_4. & (1-\bar{\lambda}_\varepsilon)\le \bar{w}_2\le 1+2\bar{h}-\bar{\lambda}_\varepsilon\end{cases} \tag{29b}$$

Note that two hinges are located at x=0 and x=L, respectively. For half of the sandwich beam, the energy dissipation rate due to the plastic bending and the axial stretching can be calculated as

$$J_{mn}/2=(M+M_m)\dot{\kappa}+N_p\dot{\varepsilon},\quad J_{mm}/2=2M_p\dot{\kappa},\quad \dot{\kappa}=\frac{\dot{W}_0}{L_0},\dot{\varepsilon}=\frac{W_0\dot{W}_0}{L_0}, \tag{30}$$

where M is the bending moment at the support, and M_m the bending moment at the mid-span.

Substituting Eqs. (28) and (29) into Eq. (30), the sandwich beam is in a membrane state with

$$f_{n1}=\begin{cases}\dfrac{\bar{\sigma}\bar{w}_1^2}{4E_1}-C_3, & 0\le \bar{w}_1\le (1-\varepsilon_D)-2\bar{Z}\\ -\dfrac{\bar{\sigma}(1-\varepsilon_D)[2\bar{w}_1-\varepsilon_D+2\bar{k}]^2}{4E_1(2-\varepsilon_D)^2}-\dfrac{\bar{\sigma}(2\bar{k}-\varepsilon_D-\bar{w}_1)[2\bar{w}_1-\varepsilon_D+2\bar{k}]}{2E_1(1-\varepsilon_D)}-C_2, & (1-\varepsilon_D)-2\bar{Z}\le \bar{w}_1\le (1-\bar{k})\\ \dfrac{(\bar{w}_1-1-2\bar{h}+\bar{k})^2}{4E_1}+\dfrac{\bar{k}(\bar{w}_1-1-2\bar{h}+\bar{k})}{2E_1}+\dfrac{(\bar{\sigma}+2\bar{h})\bar{w}_1}{2E_1}-C_1, & (1-\bar{k})\le \bar{w}_1\le 1+2\bar{h}-\bar{k}\end{cases} \tag{31a}$$

$$f_{n2}=\begin{cases}\dfrac{\bar{\sigma}\bar{w}_2^2}{4E_1(1-\varepsilon_D)}-\dfrac{(\varepsilon_D\bar{l}+\bar{\lambda}_\varepsilon-\varepsilon_D)\bar{w}_2\bar{\sigma}}{2E_1(1-\varepsilon_D)}-C_2, & 0\le\bar{w}_2\le 2\bar{z}-(1-\varepsilon_D)\\ -\dfrac{\bar{\sigma}(2\bar{w}_2-\varepsilon_D+2\bar{\lambda}_\varepsilon)^2}{4E_1(2-\varepsilon_D)^2}-\dfrac{\bar{\sigma}(\varepsilon_D\bar{l}-\bar{\lambda}_\varepsilon-\bar{w}_2)(2\bar{w}_2-\varepsilon_D+2\bar{\lambda}_\varepsilon)}{2E_1(2-\varepsilon_D)}-C_3, & \\ & 2\bar{z}-(1-\varepsilon_D)\le\bar{w}_2\le(1-\bar{\lambda}_\varepsilon)\\ \dfrac{(\bar{\sigma}+2\bar{h})\bar{w}_2}{2E_1}+\dfrac{(\bar{w}_2-1-2\bar{h}+\bar{\lambda}_\varepsilon)^2}{4E_1}-\dfrac{\varepsilon_D\bar{l}(\bar{w}_2-1-2\bar{h}+\bar{\lambda}_\varepsilon)}{2E_1}-C_4. & \\ & (1-\bar{\lambda}_\varepsilon)\le\bar{w}_2\le 1+2\bar{h}-\bar{\lambda}_\varepsilon\end{cases} \tag{31b}$$

When $\bar{w}\ge 1+2\bar{h}-\bar{\lambda}_\varepsilon$, $n=1, m=\pm C_1$ or $\pm D_4$, $f_n=\dfrac{N_pW_0+(M+M_m)}{2M_p}=\dfrac{2(\bar{\sigma}+2\bar{h})\bar{w}}{\bar{\sigma}+4\bar{h}(\bar{r}-\bar{h})}$.

At this time, considering the moment of momentum for the left half of the beam, the governing equations for the sandwich beam with large deflection are written as

$$-(\frac{GL^2}{3})\ddot{W}_0=N_pW_0+(M+M_m)=2M_pf_n. \tag{32}$$

$$\ddot{W}_0=-6M_pf_n/GL^2. \tag{33}$$

According to Eqs. (32) and (33), the responses of the sandwich beam with large deflection could be determined.

4. Numerical Examples

In order to examine the availability of the predicted model, we analyze the relationship between the face deflection and the strength of the core material. The beam geometrical parameters are: the beam aspect ratio $\bar{c}=0.3$. The sandwich beams have identical front and back faces $\hat{h}=1$, a face-sheet to core thickness ratio $\bar{h}=0.1$. For the core we have $\bar{\rho}=0.02$, and the nominal densification strain ε_D=0.85. The longitudinal strength is assumed to be equal to the ideal value $\bar{\sigma}_l=0.02$. The transverse core strength $0.001\le\bar{\sigma}_t\le 0.5$.

In the calculation, we take $\bar{\sigma}_t=0.001$ or 0.5. The loading impulse $\bar{I}=0.09$. The same as Tilbrook *et al.* [18] , when $\bar{\sigma}_t=0.001$, the deformation mechanism is in regime B (decoupled

regime with full core densification, see, Appendix B). The core is relatively weak and unable to decelerate the front face significantly and we can neglect the loading to the back face. Densification of the core occurs over the entire sandwich beam span at $t = t_{eq}$ resulting in a sudden jump of the mid-span back face velocity at the instant that the phase III commences. The support reaction is almost zero up to the core densification but displays a sudden rise when the sandwich phase of the motion commences. This support reaction continues to increase over the duration of the sandwich phase of the response. When $t = t_{eq}$, the core is full densified, the cross-section of the sandwich beam is symmetrical (as shown in Fig. 1d). When $\bar{\sigma}_t = 0.5$, the deformation mechanism is in regime A (decoupled regime with partial core densification, see, Appendix B). The front face velocity decreases linearly with the time, whist the back face velocity increases linearly until the face-sheet velocities equalize at the mid-span. When $t = t_{eq}$, the core is partial densified, the cross-section of sandwich beam is asymmetric (as shown in Fig. 1b).

Figures 8 and 9 show the comparison of the predicted results obtained by the present model and that of Tilbrook *et al.* [18] , as well as the numerical ones from FE simulation. In our modeling, the velocities of the front and back beams are coincided well with those given by FE simulation. The velocity of the front beam, predicted by Tilbrook *et al.* [18] , is larger than those given by FE simulation. The comparison indicates that our model in treatment of the core deformation is reasonable and could well describe the dynamic responses of sandwich beams under an impulse impact. Generally, considering the utility of the model, the average treatment (σ_m, see, Eq. 12) is reasonable and acceptable.

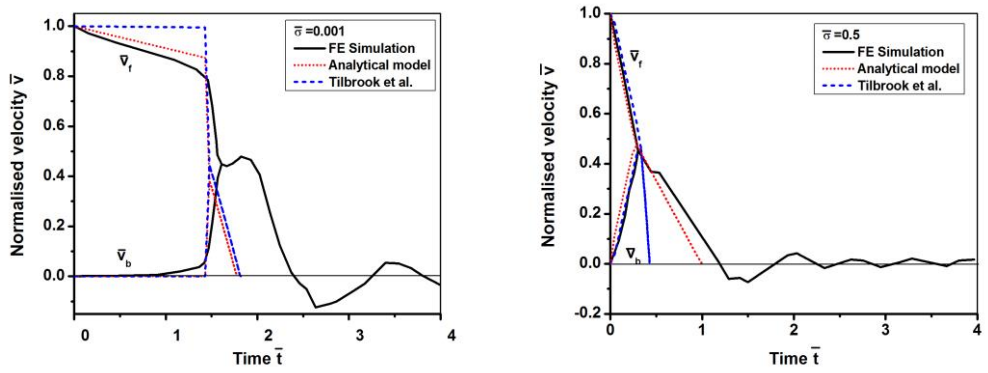

Fig. 8 Analytical and FE predictions of the time histories of the mid-span velocities of front and back face-sheets.

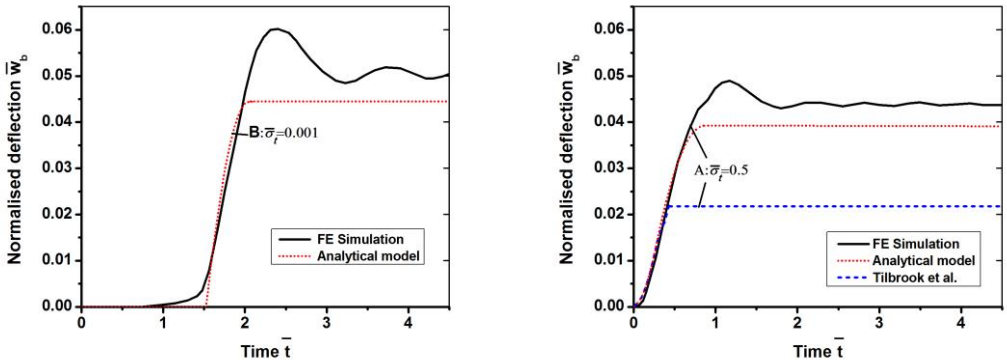

Fig.9 Analytical and FE predictions of time histories of the normalized mid-span deflection of back face sheet $\bar{w}_b$.

Fig. 10 gives the variation of the normalized mid-span velocity and mid-span deflection with respect to the time with the same core strength but selected values of the loading impulse. Seen as Fig. 10a, the deformation mechanisms are all in regime B (decoupled regime with full core densification). The mid-span velocity of the sandwich beam changes to another mode as the deflections exceed $1-\varepsilon_D$ because the variation of the axial force N and the bending moment M at this time. In Fig. 10b, for small impulse impacting, the mid-span deflection is less than the thickness of the sandwich beam. The deformation of the sandwich beam is coupling response dominated. Along with the increase of the loading impulse, the deformation of the sandwich beam is overall deformation stage dominated, and the time t_{eq} is decreased. It is seen clearly that on the time-scales, we can predict the front face and back face velocities and mid-span back face

deflections.

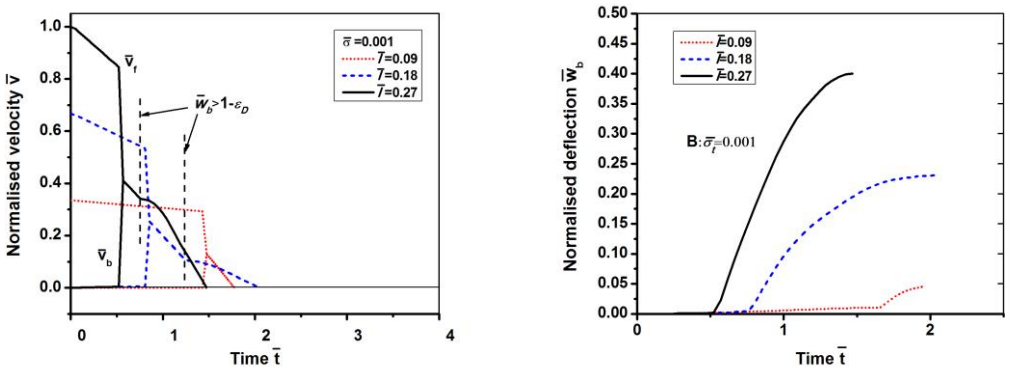

Fig. 10 Analytical predictions of the time histories of the normalized mid-span front and back face-sheet velocities and back face deflection for sandwich beams under different impulses.

5. Conclusions

The response of fully clamped slender sandwich beams with changed cross-sectional neutral axis struck by an impulse is investigated in this paper. Under the high-speed impact, densification regions of the core are changed with the time, resulting in the variation of the neutral axis of the sandwich beam. The cross section of sandwich beam changes from asymmetry to symmetry along with the core deformation. Considering the inhomogeneity of the core deformation, the yielding criteria for sandwich beams are presented, which is available for the sandwich beams under high velocity impact, as well as the low velocity impact and quasi-static loading.

Based on the proposed dynamic yielding criteria, the governing equations for a sandwich beam under blasting loading are obtained by introduction the membrane factor to accounting for the large deflection. It is clear that the compressive stress σ_m of the core induced by high velocity impact should be considered in large deflection analysis, which plays an important role in the coupling response. The comparison between the theoretical prediction and numerical simulation indicates the availability and accuracy of the present model.

ACKNOWLEDGEMENTS

The financial supports from the Fundamental Research Funds for the Central University (No. 2014yjs109), the National Science Foundation of China (No. 11272046,), 111 project, and 973 Program (No. 2015CB057800) are acknowledged.

Appendix A

End of core compression

After the core compression ends, the face sheets move co-operatively and sandwich action dominates the response. Following Fleck and Deshpande [1], we assume that sandwich action commences at the time t_{eq} when core compression ends, that is, the core has densified at the supports, or the front and back face-sheet velocities are equal at the mid-span, whichever occurs first.

There are three cases:

Case I: $\sigma_t > 3(\sigma_Y h_b^2 / L^2)$

Equalizations of the velocities of the faces in this case can occur in the following three scenarios: (a) during phase I of the back face; (b) during phase II of the back face; or (c) after motion of the back face has ceased.

Case I (a): Core compression ends during phase I of the back face motion. We obtain the time

$$\theta_I = \frac{v_0 m_b m_f}{\sigma_m m_b + \sigma_t m_f} \tag{A1}$$

For this solution to be valid we require that $\theta_I < t_I$

$$t_{eq} \equiv \min(\theta_I, t_D) \le t_I \tag{A2}$$

If this inequality is not met, then core compression continues into phase II of the back face motion.

$$w_b^{eq} = \frac{\sigma_t}{2m_b} t_{eq}^2 \tag{A3}$$

The core compression at mid-span and at the supports then follow as

$$\varepsilon_m = \frac{1}{c}[v_0 t_{eq} - \frac{\sigma_t}{2m_f} t_{eq}^2 - w_b^{eq}] \tag{A4a}$$

$$\varepsilon_s = \frac{1}{c}[v_0 t_{eq} - \frac{\sigma_t}{2m_f} t_{eq}^2] \tag{A4b}$$

Case I (b): Core compression ends during phase II of the back face motion.

$$v_0 - \frac{\sigma_m}{m_f} = v_b^I \cos[\omega(\theta_{II} - t_I)] + \frac{4M_b}{N_b}\omega \sin[\omega(\theta_{II} - t_I)] \tag{A5a}$$

$$t_I < t_{eq} \equiv \min(\theta_{II}, t_D) \le t_{bs} \tag{A5b}$$

If neither inequality (2) nor (5b) is satisfied, then core compression continues after the back face has arrested.

Case I(c): Core compression ends after the arrest of the back face.

$$\theta_{III} = \frac{m_f v_0}{\sigma_m} \tag{A6a}$$

$$t_{eq} \equiv \min(\theta_{III}, t_D) > t_{bs} \tag{A6b}$$

Case II: $\sigma_Y h_b^2 / L^2 < \sigma_t \le 3(\sigma_Y h_b^2 / L^2)$

$$v_0 - \frac{\sigma_m}{m_f}\theta = \omega(\frac{\sigma_t L^2 - 4M_b}{2N_b}) \sin \omega\theta \tag{A7a}$$

$$0 < t_{eq} \equiv \min(\theta, t_D) \le t_{bs} \tag{A7b}$$

Case III: $\sigma_t \le \sigma_Y h_b^2 / L^2$

Recall that in this case the transverse compressive strength of the core is insufficient to initiate deformation in the back face. Equalizations of the front and back face velocities occurs at t_{eq} either if the motion of the front faces ceases or (b) if core densification occurs. The midspan back face deflection w_b and velocity v_b are identically zero over the duration $0 \le t \le t_{eq}$.

Appendix B

Regimes of behavior

The response regimes of the sandwich beam can be defined by comparing various time-scales and summarized as:

Regime A: Decoupled response with partial core densification:

$t_{eq} < t_D$ and $t_{eq} < t_{bd}$

Regime B: Decoupled regime with full core densification:

$t_{eq} = t_D$ and $t_{eq} < t_{bd}$

Regime C: Decoupled regime with full core densification:

$t_{eq} < t_D$ and $t_{eq} > t_{bd}$

Regime D: Coupled response with full core densification:

$t_{eq} = t_D$ and $t_{eq} > t_{bd}$

References

[1] Fleck NA, Deshpande VS. The resistance of clamped sandwich beams to shock loading. ASME J Appl Mech 2004;71:386-401.

[2] Ashby MF, Evans AG, Fleck NA, Gibson LJ, Hutchinsion JW, Wadley HNG. Metal foams: a design guide. Oxford: Butterworth-Heinemann; 2000.

[3] Tan P, Harrigan J, Reid S. Inertia effects in uniaxial dynamic compression of a closed cell aluminium alloy foam. Mater Sci Tech-lond 2002;18:480-488.

[4] Lopatnikov SL, Gama BA, Jahirul Haque M, Krauthauser C, Gillespie Jr JW, Guden M, Hall IW.

Dynamics of metal foam deformation during Taylor cylinder–Hopkinson bar impact experiment. Compos Struct 2003;61:61-71.

[5] Lopatnikov SL, Gama BA, Haque MJ, Krauthauser C, Gillespie Jr JW. High-velocity plate impact of metal foams. Int J Impact Eng 2004;30:421-445.

[6] Radford DD, Deshpande VS, Fleck NA. The use of metal foam projectiles to simulate shock loading on a structure. Int J Impact Eng 2005; 31 (9):1152–1171.

[7] Tilbrook M, Radford DD, Deshpande VS, Fleck NA. Dynamic crushing of sandwich panels with prismatic lattice cores. Int J Solids Struct 2007;44:6101-6123.

[8] Barnes AT, Ravi-Chandar K, Kyriakides S, Gaitanaros S. Dynamic crushing of aluminum foams: Part I – Experiments. Int J Solids Struct 2014;51:1631-1645.

[9] Gaitanaros S, Kyriakides S. Dynamic crushing of aluminum foams: Part II – Analysis. Int J Solids Struct 2014;51:1646-1661.

[10] Qin QH, Wang TJ. Analytical solution for the large deflection of fully clamped metallic foam sandwich beam. Adv Mater Res 2008;33:559-566.

[11] Qin, QH, Wang TJ. An analytical solution for the large deflections of a slender sandwich beam with a metallic foam core under transverse loading by a flat punch. Compos Struct 2009;88:509-518.

[12] Qin, QH, Wang TJ. A theoretical analysis of the dynamic response of metallic sandwich beam under impulsive loading. Eur J Mech-A/Solids 2009;28:1014-1025.

[13] Qin QH, Wang TJ, Zhao SZ. Large deflections of metallic sandwich and monolithic beams under locally impulsive loading. Int J Mech Sci 2009;51:752-773.

[14] Qin QH, Zhang JZ, Wang ZJ, Wang TJ. Large deflection of geometrically asymmetric metal foam core sandwich beam transversely loaded by a flat punch. Int J Aerosp Lightweight Struct 2011;1:23-46.

[15] Wang ZJ, Qin QH, Wang TJ. Low-velocity impact response of geometrically asymmetric slender sandwich beams with metal foam core. Compos Struct 2013;98:1–14.

[16] Jones N. Structural Impact. Cambridge: Cambridge University Press ; 1989.

[17] Liang Y, Spuskanyuk AV, Flores SE, Hayhurst DR, Hutchinson JW, McMeeking RM, Evans AG. The response of metallic sandwich panels to water blast. J Appl Mech-t Asme 2007;74:81-99.

[18] Tilbrook M, Deshpande V, Fleck N. The impulsive response of sandwich beams: Analytical and numerical investigation of regimes of behaviour. J Mech Phys Solids 2006;54 (11):2242-2280.

[19] Yu TX, Stronge WJ. Large deflections of a rigid-plastic beam-on-foundation from impact. Int J Impact Eng 1990;9:115–126.

A list of figure captions:

Fig. 1 Original and deformed cross-sections of the sandwich beam.

Fig. 2 Typical dynamic stress-strain curves for the foam. The red line corresponds to rigid ideally-plastic-locking model.

Fig.3 Distributions of the strain and stress on the cross-section of multilayer beam under bending moment and axial force.

Fig. 4 Dynamic yield surfaces for the compressed sandwich beam along with the compression.

Fig. 5 Geometry of the sandwich beam and schematic of the problem under consideration.

Fig. 6 A sketch summarizing the model of the sandwich beam subject to impulse loading.

Fig. 7 (a) Velocity profile of the back face in phase I, (b) a free-body diagram of the left half back beam in phase I; (c) velocity profile of the back face in phase II, and (d) a free body diagram of the left half back beam in phase II; (e) velocity profile of the sandwich phase, and (f) a free body diagram of the half beam.

Fig. 8 Analytical and FE predictions of the time histories of the mid-span velocities of front and back.

Fig. 9 Analytical and FE predictions of time histories of the normalized mid-span deflection of back face sheet $\bar{w}_b$.

Fig. 10 Analytical predictions of the time histories of the normalized mid-span front and back face-sheet velocities and mid-span back face deflection for sandwich beams under different impulses.

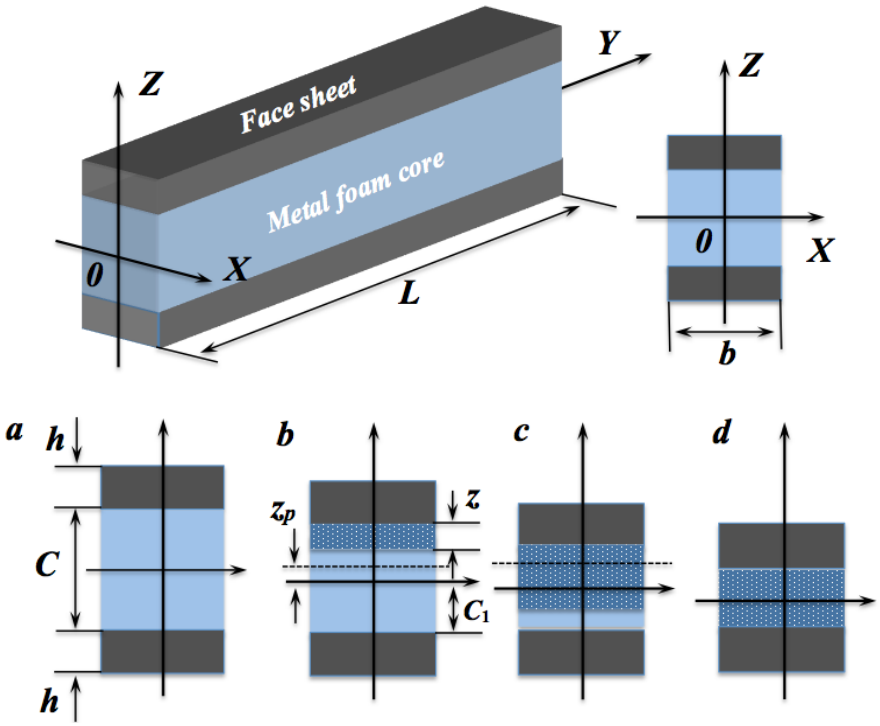

Fig. 1. Original and deformed cross-sections of the sandwich beam.

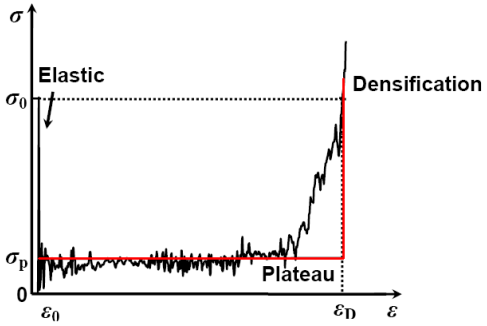

Fig. 2 Typical dynamic stress-strain curves for the foam. The red line corresponds to rigid ideally-plastic-locking model.

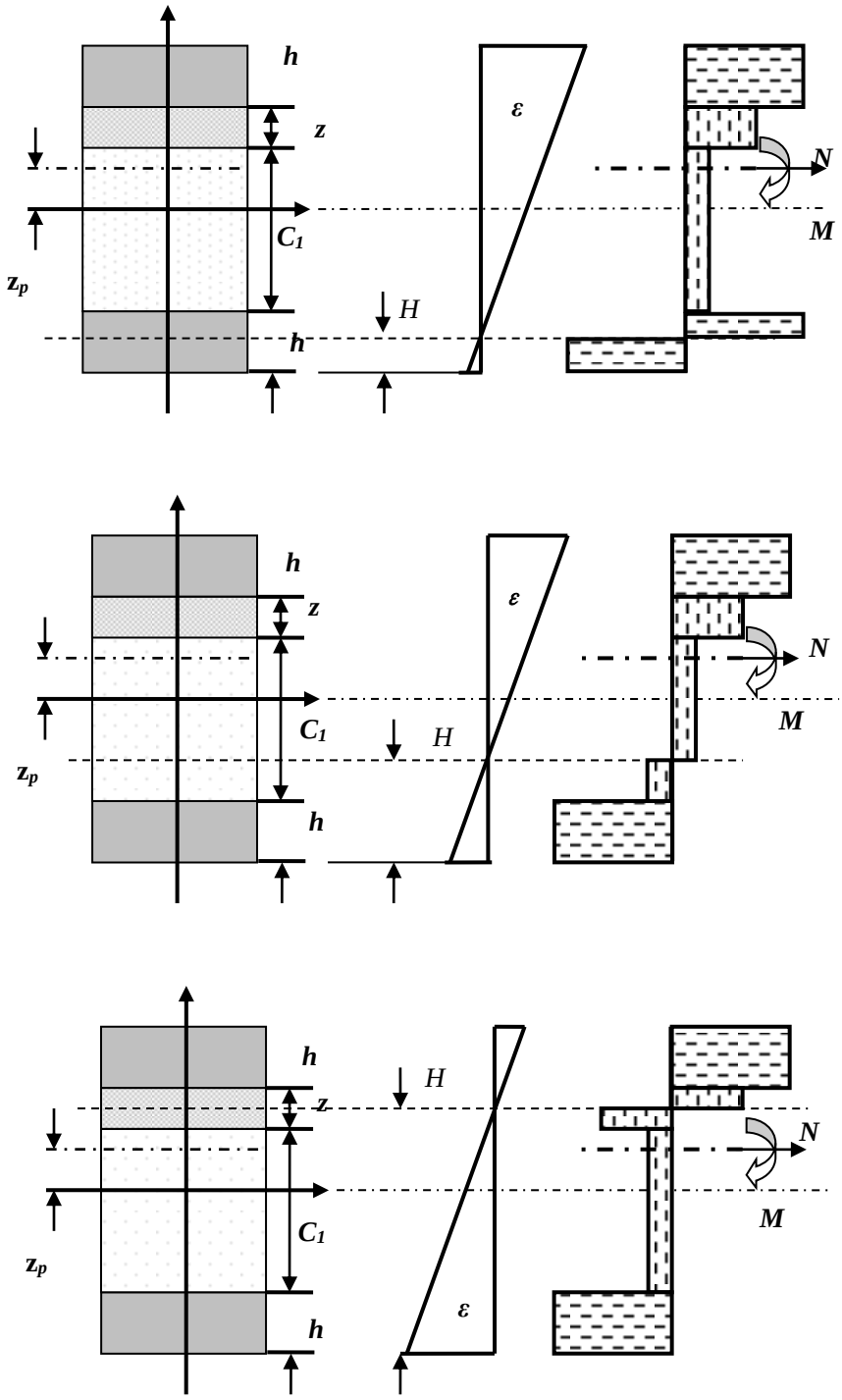
h
z
C1
zp
H
h
ε
N
M
h
z
C1
zp
H
h
ε
N
M
h
H
z
C1
zp
h
ε
N
M

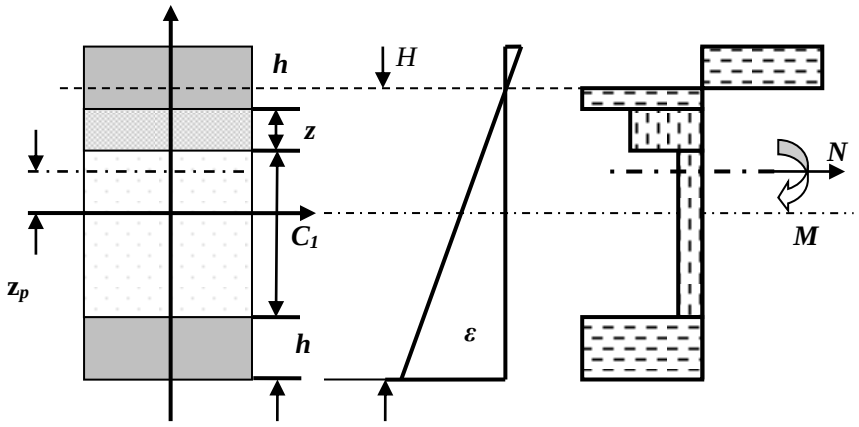

Fig.3 Distributions of the strain and stress on the cross-section of multilayer beam under bending moment and axial force.

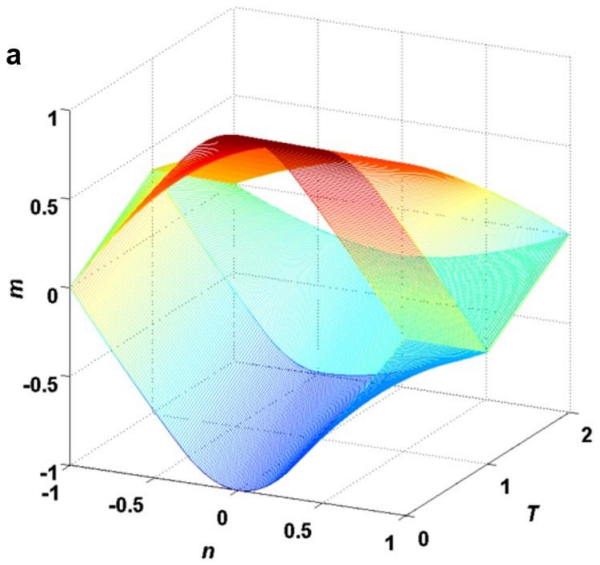

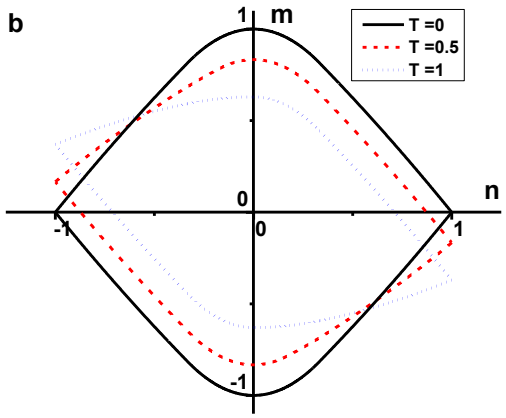

Fig. 4 Dynamic yield surfaces for the compressed sandwich beam along with the compression.

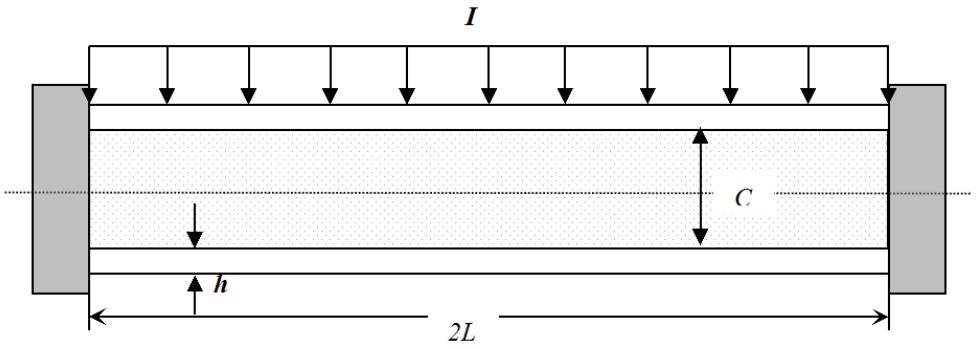

Fig. 5. Geometry of the sandwich beam and schematic of the problem under consideration.

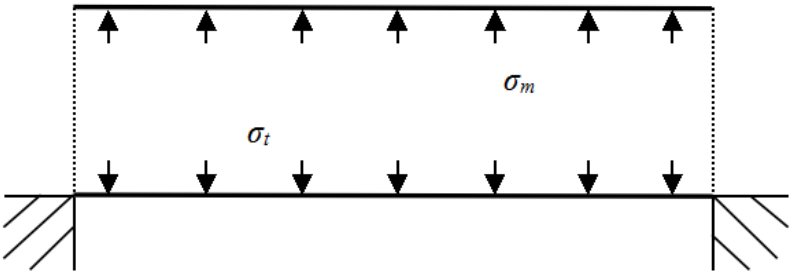

Fig. 6. A sketch summarizing the model of the sandwich beam subject to impulse loading.

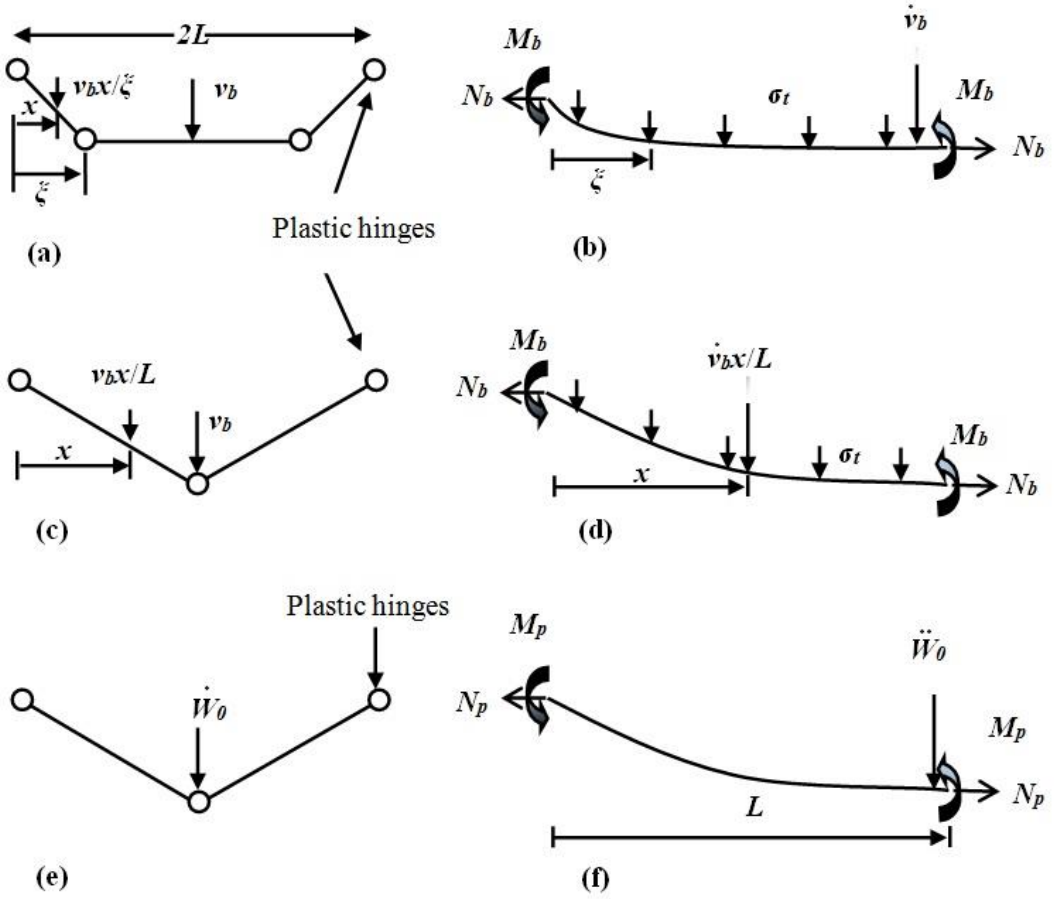

Fig. 7 (a) Velocity profile of the back face in phase I, (b) a free-body diagram of the left half back beam in phase I; (c) Velocity profile of the back face in phase II, and (d) a free body diagram of the left half back beam in phase II; (e) Velocity profile of the sandwich phase, and (f) a free body diagram of the half beam.

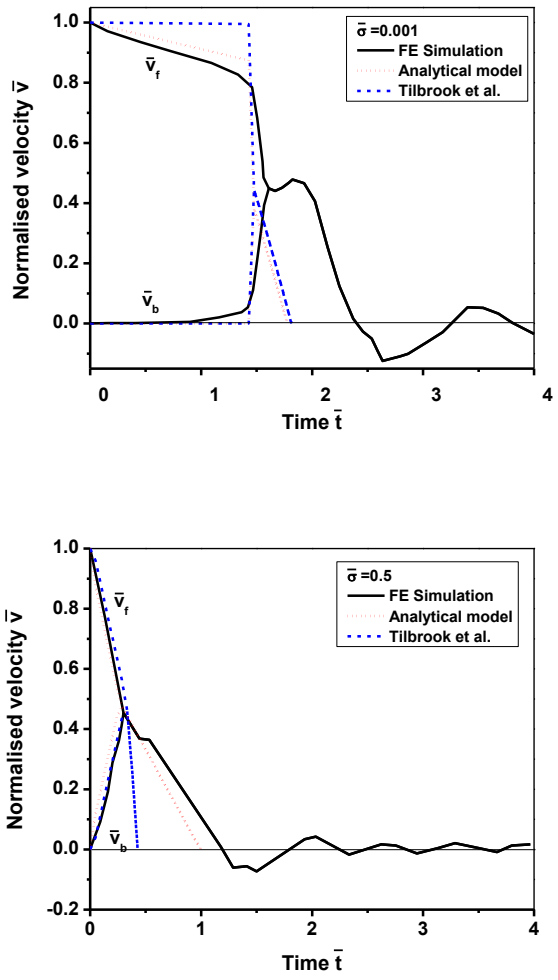

Fig. 8 Analytical and FE predictions of the time histories of the mid-span velocities of front and back.

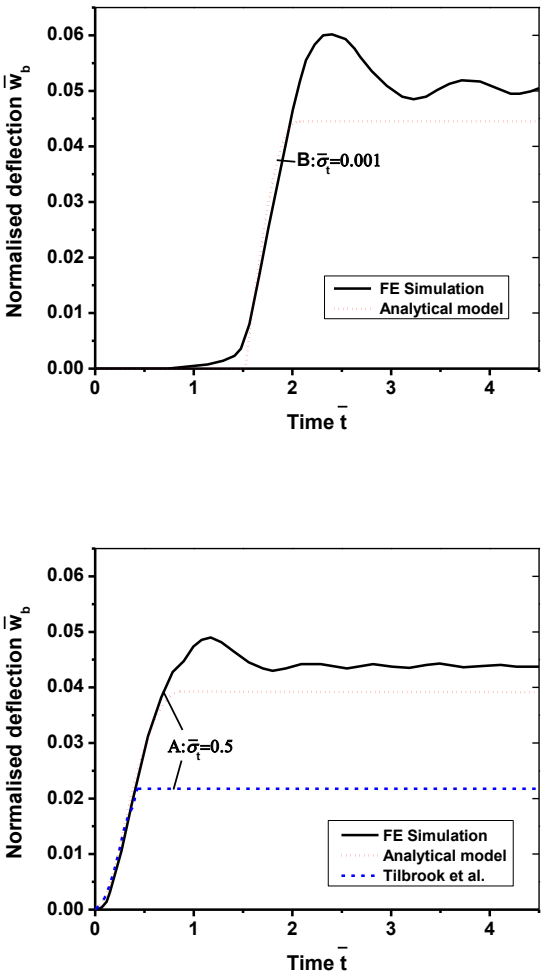

Fig.9 Analytical and FE predictions of time histories of the normalized mid-span deflection of back face sheet $\bar{w}_b$.

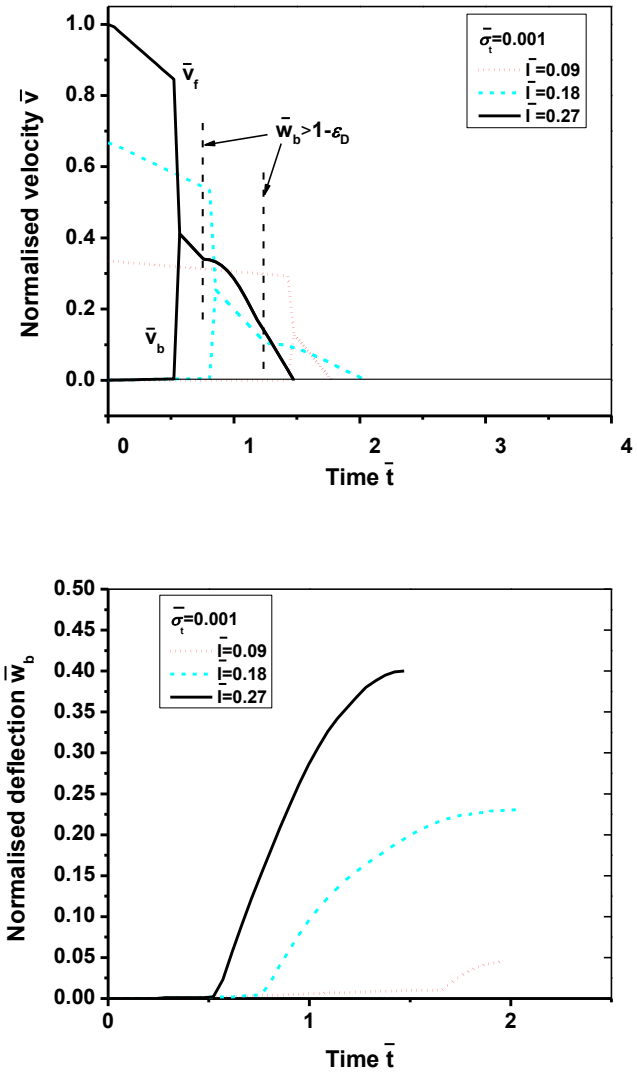

Fig. 10 Analytical predictions of the time histories of the normalized mid-span front and back face-sheet velocities and mid-span back face deflection for sandwich beams under different impulses.